Priority Report

Cancer Research

Glutamate-Weighted Chemical Exchange Saturation Transfer Magnetic Resonance Imaging Detects Glutaminase Inhibition in a Mouse Model of Triple-Negative Breast Cancer

Rong Zhou, Puneet Bagga, Kavindra Nath, Hari Hariharan, David A. Mankoff, and Ravinder Reddy

Abstract

Glutamate is an important metabolite of glutaminolysis, a metabolic pathway used by many aggressive cancers, including triple-negative breast cancer (TNBC). With the exception of the brain, *in vivo* detection of glutamate in tissues using ^{1}H magnetic resonance spectroscopy (MRS) is challenging. Compared with MRS, glutamate-weighted chemical exchange saturation transfer MR imaging (GluCEST MRI) offers a more sensitive detection mechanism that is free of glutamine interference. Here, we developed a robust, highly repeatable GluCEST MRI protocol in mice bearing human TNBC xenografts and treated with a potent glutaminase inhibitor, CB-839. In paired studies, treatment with CB-839 for 2 days reduced the GluCEST asymmetry value compared with baseline ($P < 0.05$, $n = 10$). The absolute change of the GluCEST asymmetry value was −2.5 percent points after CB-839 treatment versus +0.3 after vehicle ($P < 0.01$). Correspondingly, treatment with CB-839 reduced tumor glutamate concentrations by 1.5 mmol/L, consistent with prior calibration between changes of the GluCEST value versus tissue glutamate concentration; CB-839, however, did not change tumor intracellular pH. These results demonstrate in a mouse model of breast cancer the utility of GluCEST MRI to detect the early response to glutaminase inhibition.

Significance: A sensitive method enables noninvasive detection of tumor response to inhibitors of glutamine metabolism. *Cancer Res; 78(19); 5521–6. ©2018 AACR.*

Introduction

Glutamate plays an important role in cancer metabolism, especially in glutaminolysis pathway, where cellular glutamate level is associated with the catabolism of glutamine by mitochondrial glutaminase, *GLS*, activity (Fig. 1A). Recent discoveries in cancer metabolism have revealed that glutaminolysis is activated in many aggressive forms of human cancers, including the triple-negative breast cancers (TNBC). This provides strong rationale to target the cancer-specific metabolic signature. As the first and rate-limiting enzyme of glutaminolysis, inhibition of *GLS* activity can effectively block glutamine's utilization for macromolecular synthesis and energy (1, 2). Developing *GLS*-targeted strategy is especially important for TNBC, which has higher recurrence rate after surgical removal of the primary tumor and is not responsive to endocrine (e.g., tamoxifen) or HER2-targeted therapies. Several small-molecule inhibitors of *GLS* were developed and a highly potent and selective *GLS* inhibitor, CB-839, is undergoing clinical trials in patients with glutaminolytic cancers, including TNBC (2, 3). In TNBC tumors that exhibit high *GLS* and low glutamate synthase activity (3, 4), previous studies revealed a direct proportional relationship between *GLS* activity and cellular glutamate concentration. Consequently, change in the tumor glutamate level could be a measurable indicator of *GLS* inhibition.

Noninvasive measurement of tissue glutamate level by *in vivo* ^{1}H magnetic resonance spectroscopy (MRS) is established in the brain, which has the highest glutamate concentration (6∼12.5 mmol/L) of all tissues (5). In non-neuronal tissues, however, *in vivo* ^{1}H MRS is not feasible to assess glutamate level even with the sophisticated acquisition and post-processing methods (6) owing to (i) much lower glutamate concentration than the brain, (ii) interfering signals from lipids, and (iii) overlapping with glutamine resonance peaks. Therefore, a more sensitive glutamate detection method that is free of the above limitations is highly desirable.

Glutamate is among a few endogenous metabolites that exhibit the chemical exchange saturation transfer (CEST) effect (7), providing an amplification mechanism that allows indirect detection of low concentration solute pool (such as glutamate). Glutamate-weighted CEST (GluCEST) MRI demonstrates greater than 100-fold increase in sensitivity over

Department of Radiology, Perelman School of Medicine, University of Pennsylvania, Philadelphia, Pennsylvania.

Note: Supplementary data for this article are available at Cancer Research Online (http://cancerres.aacrjournals.org/).

R. Zhou and P. Bagga contributed equally to the article.

Corresponding Authors: Rong Zhou, University of Pennsylvania, John Morgan 198, 3620 Hamilton Walk, Philadelphia, PA 19104. Phone: 215-746-8787; Fax: 215-573-2255; E-mail: rongzhou@upenn.edu; and Ravinder Reddy, University of Pennsylvania, B1-Stellar-Chance labs, 422 Curie Blvd., Philadelphia, PA 19104. Phone: 215-898-5708; Fax: 215-573-2113; E-mail: krr@pennmedicine.upenn.edu

doi: 10.1158/0008-5472.CAN-17-3988

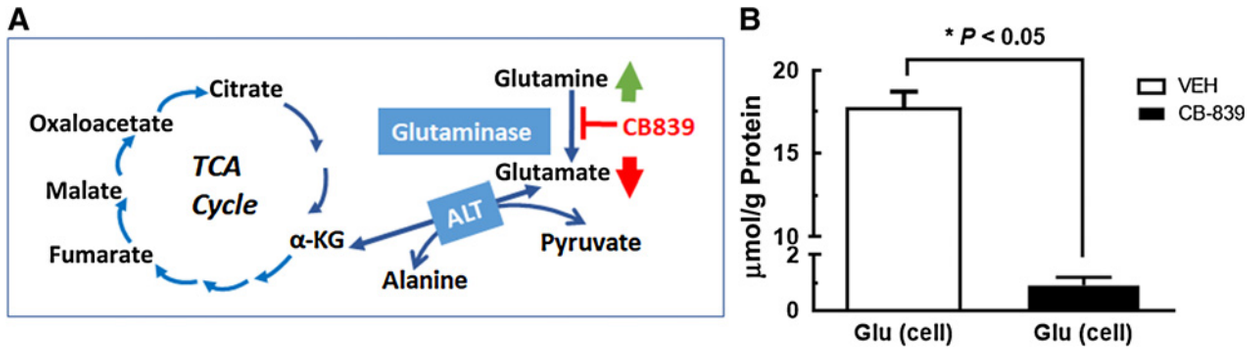

Figure 1.

Metabolic pathway of glutaminolysis in cancer and cellular glutamate level in TNBC cells after vehicle (VEH) or GLS inhibitor (CB-839) treatment. **A,** Mitochondrial glutaminase (GLS; kidney type) catalyzes the conversion of glutamine to glutamate, the first and rate-limiting step of glutaminolysis pathway. **B,** Cellular glutamate concentrations (µmol/g protein) after TNBC cells (HCC1806) were exposed to the vehicle (0.01% DMSO in culture media; $n = 2$) or 1 µmol/L CB-839 (in same amount of DMSO; $n = 2$) for 24 hours, followed by extraction of aqueous metabolites (Supplementary Methods).

^{1}H MRS detection of glutamate in the brain (8). GluCEST has shown great utility in several neurological/psychiatric applications (9–11). However, its ability to assess the pharmacodynamics of drugs targeting cancer glutaminolysis has not been examined.

Radio-labeled glutamate analogs detectable by PET, such as ^{18}F-fluoroglutamate (12) or ^{18}F-FSPG (13), are very sensitive but their signals represent cellular glutamate transporter activity rather than the endogenous glutamate level in the tissue. To our knowledge, GluCEST MRI is the only method that has the sensitivity potentially suitable for noninvasively assessing changes in tumor glutamate level. On the basis of the mechanistic link between cellular glutamate level and *GLS* activity in TNBC, we hypothesized that a reduction of overall GluCEST signal would be observed in TNBC tumors responding to *GLS* inhibitor. To test this hypothesis, we conducted the first feasibility study of GluCEST MRI as a therapeutic marker of *GLS* inhibitor.

Materials and Methods

Human TNBC cell line, HCC1806 (ATCC), exhibiting high *GLS* activity (3), was authenticated using the Short Tandem Repeat DNA profiling and was tested to be free of *Mycoplasma* by agar culture and Hoechst DNA staining. Cells within 50 passages were used. *GLS* inhibitor, CB-839 (Calithera Biosciences) was obtained via a material transfer agreement.

Tumor inoculation, treatment, and imaging schedule, quantification of aqueous metabolites concentration in tumor tissue and cell extracts, *in vivo* measurement of tumor intracellular pH by ^{31}P MRS are described in the Supplementary Methods. Animal studies were approved by local Institutional Animal Care and Use Committee.

In vivo GluCEST MR imaging was performed on a 9.4 Tesla horizontal bore MR spectrometer (Agilent). A custom-built slotted-tube cylindrical resonator (13-mm inner diameter ×16.5-mm height) tuned to ^{1}H was installed underneath a flat plastic platform on which the mouse was lying on its side with the flank tumor fit inside the resonator cylinder. The mouse was anesthetized with 1% to 2% isoflurane (mixed in air at 1 L/min) whereas the respiration and temperature were monitored, and the rectal temperature was maintained at 37 ± 0.2°C by warm air (SA Inc.).

Homogeneity of the static magnetic field (B_0) was improved by shimming of the entire tumor using the point-resolved spectroscopy (PRESS) technique. For imaging, a single, 10-mm thick slice was planned to include the entire tumor (<10 mm in any dimension). To minimize the effect of respiration motion, the slice direction was parallel to the diaphragm motion. This slice was used for acquiring the B_0 and radiofrequency field (B_1) map (14), GluCEST and T_2-weighted (T2W) gradient echo images with a matrix size of 128 × 128 over a field of view (FOV) of 25 × 25 mm^2. B_0 map was acquired using the Water Saturation Shift Referencing (WASSR) technique (15): A saturation pulse of 400 msec duration was applied with B_1 of 0.3 µT and Δω in the range of −1 to +1 ppm with 0.1 ppm increment.

CEST images were acquired using a saturation pulse consisting of 4 square pulses of 250 msec each with a 4 µsec interpulse-delay and a 64-segment GRE readout (segment TR/TE = 6.7/3.4 msec). The B_1 was optimized to 5.9 µT (250 Hz) to adequately saturate the amine protons on glutamate (9) and was applied with offset frequencies of ±2.5, ±2.75, ±3, ±3.25, ±3.5 ppm in reference to the bulk water. For each offset frequency, four acquisitions were executed with an 8-sec interval to allow T_1 recovery. Within-subject variability was assessed by test-retest study, where two GluCEST imaging sessions were performed on the same mice in a single same day and the mice were recovered from the anesthesia and returned to the cage during the interval.

CEST images were first corrected for B_0 and B_1 inhomogeneity (8). On the basis of the B_0 and B_1 map, the tumor region in which the B_0 and relative B_1 were within [−0.4 to 0.4] ppm and [0.8–1.2], respectively was processed to generate pixel-wise GluCEST asymmetry map using Eq. A (7), where the MTR_{asymm} is normalized to the signal losses by direct water saturation and magnetization transfer contrast at -Δω:

$$GluCEST_{asym(\Delta\omega=3\,ppm)} = \frac{M_{sat(-\Delta\omega)} - M_{sat(+\Delta\omega)}}{M_{sat(-\Delta\omega)}} \times 100\% \qquad (A)$$

The M_{sat} ($\pm\Delta\omega$) are images obtained with saturation at a '+' or '−' offset frequency (Δω) to the water resonance. The GluCEST

asymmetry value is presented in percent point. In addition to the GluCEST scans, complete MTR_{asymm} analysis was applied on one animal before and after CB-839 treatment. For this, all the acquisition parameters were the same as GluCEST except the $\Delta\omega$ was ranged [−5 to +5]ppm with the step size of 0.2 ppm. The pre- and post-treatment data was processed using a MATLAB script to generate the z-spectrum and MTR_{asymm} from the tumor region.

Statistical analysis

Data are presented as mean ± standard deviation (SD) unless specified otherwise. Repeatability was evaluated by Coefficient of variation (CV = mean/SD). Statistical significance was evaluated by two-sided Student *t* tests with $\alpha = 0.05$ using GraphPad 6.

Results

To assess the extent of glutamate reduction induced by GLS inhibition (Fig. 1A), we first measured the absolute glutamate concentration in TNBC cells using high-resolution ^{1}H MRS of aqueous extracts. We found that CB-839 induced a profound reduction of cellular glutamate concentration: glutamate level in vehicle (VEH)-treated cells was approximately 19-fold of CB-839–treated cells (Fig. 1B), confirming that cellular glutamate level is sensitive to inhibition of GLS activity.

The T2W image and GluCEST map (overlaid on T2W image) from two CB-839 treated mice are shown in Fig. 2A–D, revealing a clear reduction in GluCEST value in response to the GLS inhibition. In contrast, there was no change of average GluCEST value after VEH treatment (Fig. 2E–H). The B_0 and B_1 maps and their mean values indicate good B_0 and B_1 homogeneity obtained at baseline and post-treatment scans (Supplementary Fig. S1A and S1B). The tumor region that meets both B_0 and relative B_1 homogeneity cutoff accounted for averagely 85% of the entire tumor volume. Pixel-wise GluCEST was measured from this region to derive GluCEST map. This protocol led to robust test-retest repeatability: The SD of tumor GluCEST value is 0.3 percent point and CV (SD/mean) is 0.016. Therefore, a measured change of GluCEST value ≥ 1.5 percent points (i.e., 5 × SD) would be highly reliable (not by chance).

Paired GluCEST values were obtained at baseline and post-treatment (Fig. 3A): CB-839 induced a reduction of GluCEST in 9 out 10 mice ($P < 0.05$ comparing baseline vs. post), whereas little change detected in VEH-group ($n = 7$). On average, CB-839 induced an absolute 2.5 percent points decrease of GluCEST value whereas VEH led to a 0.28 percent point increase. Compared with the baseline, GluCEST was decreased 11.3% after CB-839 but increased 1.6% after VEH treatment ($P < 0.001$, Fig. 3B). Analyses of z-spectra obtained before and after CB-839 treatment were consistent with the extent of MTR_{asymm} reduction at approximately 3 ppm (Supplementary Fig. S2). Tumor size did not change

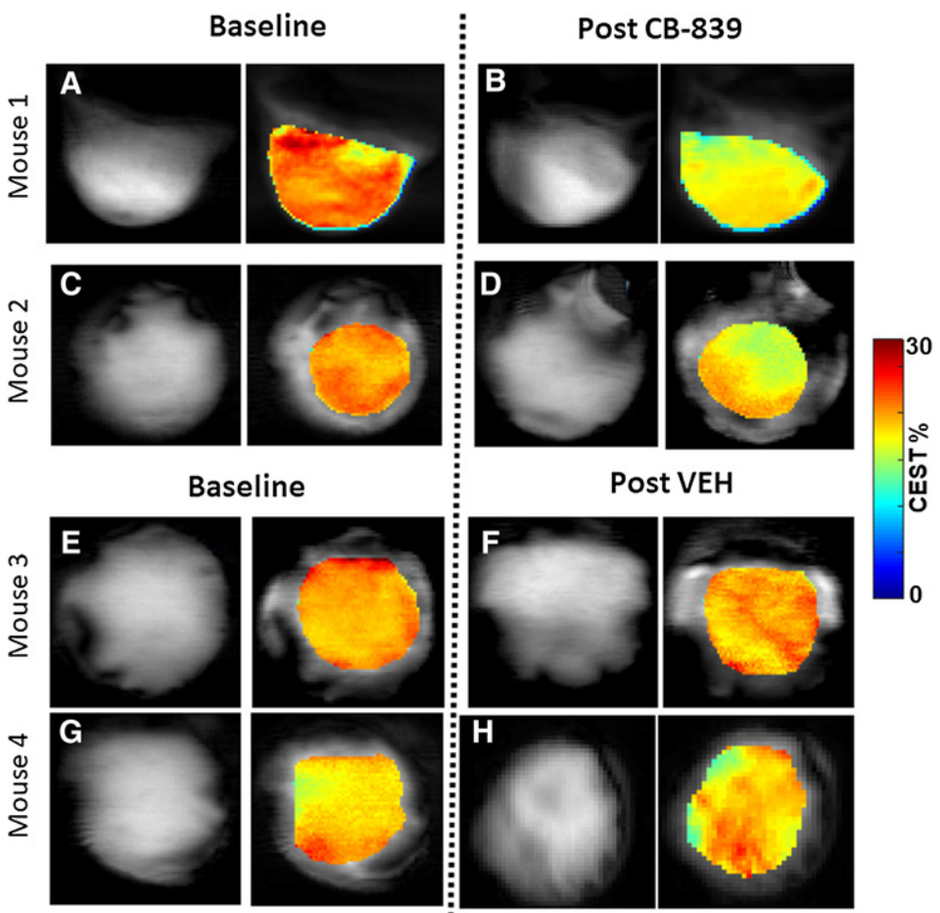

Figure 2.
In vivo GluCEST MRI of the tumor. Representative T2W anatomic image and GluCEST map (overlaid on T2W image) at baseline and post-treatment from two CB-839–treated mice (**A–D**) and two VEH-treated mice (**E–H**). The GluCEST map (in color scale) includes the region that meets both B_0 and B_1 homogeneity criteria (see text), thus it is slightly smaller than the tumor delineated on the T2W image (grayscale). Note that the single slice includes the entire tumor, although the tumor appears slightly different in the baseline and post-treatment image due to the positioning of the mice.

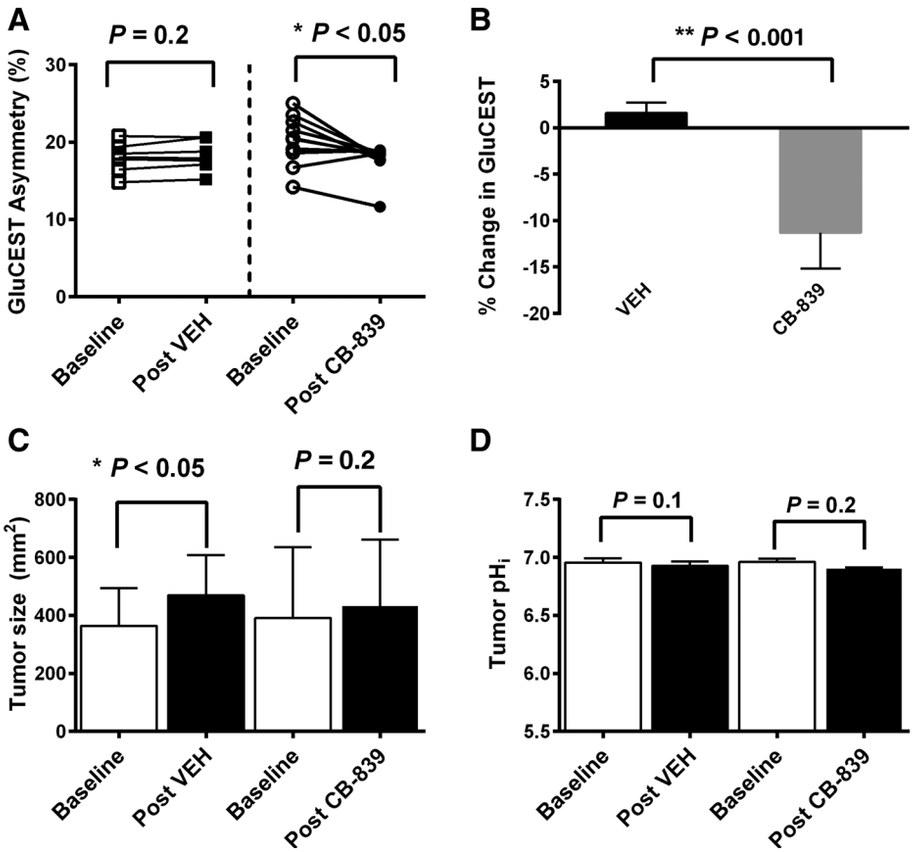

Figure 3.
The GluCEST MRI value, tumors size, and intracellular pH in response to glutaminase inhibitor treatment. **A,** Paired GluCEST MRI values pre and post VEH ($n = 7$) or CB-839 ($n = 10$) treatment. **B,** The percentage of change of the GluCEST value (= post/pre-1). Sample size is the same as in **A**. **C,** Tumor size pre- and post-treatment (the same cohorts of mice as in **A**). **D,** In a separate cohort, intracellular pH of tumor pre- and post-treatment ($n = 3$ for each treatment arm).

significantly after the short course of CB-839 treatment whereas it was increased significantly in the VEH group (Fig. 3C). Importantly, the 2-day exposure to the *GLS* inhibitor had little effect on tumor pH_i estimated by *in vivo* ^{31}P MR spectroscopy: pH_i was 6.96 at baseline, 6.90 after CB-839 and 6.93 after VEH treatment (Fig. 3D).

To assess the potential contribution of tumor glutamate and other metabolites to the GluCEST MRI signal, tumor tissues from mice treated by CB-839 or VEH (the same dose/duration as the imaging study) were harvested by freeze-clamping and extracted for ^1H MRS (detailed in Supplementary Informationr; ref. 16). Representative ^1H MR spectra of the tumor extract are shown for VEH (Fig. 4A) and CB-839–treated mouse (Fig. 4B). Compared with the VEH controls, CB-839–treated group had a 3-fold lower glutamate concentration ($P = 5.4 \times 10^{-5}$, Fig. 4C). Besides Glu, other ^1H MRS quantifiable major metabolites were listed in Supplementary Table S1, which revealed a moderate decrease of tumor alanine (9.7%) in response to CB-839 treatment but no significant change in choline or lactate level. This suggests that commonly used breast cancer markers (choline and lactate) detectable by *in vivo* ^1H MRS are not sensitive for early detection of GLS inhibition.

Discussion

GLS inhibitors represent a new category of drugs, which are directed at specific metabolic signatures of the tumor, and unlike chemotherapy, they do not induce rapid cell death or tumor shrinkage (3). Hence, their therapeutic effect, especially early responses of the tumor cannot be sufficiently evaluated by the tumor size. Meanwhile, other established markers for breast cancer therapy such as FDG-PET, lactate and/or choline detected by *in vivo* MRS are not sensitive to *GLS* inhibition (Supplementary Table S1). In this study, we demonstrated the feasibility of GluCEST MRI to detect early therapeutic responses of tumor to GLS inhibition. CEST MRI of endogenous metabolites including the amide proton transfer (APT; ref. 17) and GluCEST has a great potential to reach the clinic because it does not need any exogenous contrast media and can be performed on the existing 3T (for APT) and high field 7T (for GluCEST) MRI scanners (18).

Glutamate-weighted nature of the GluCEST value is supported by our experimental condition and results. First, APT and glutamine have negligible contribution because the B_1 saturation required for GluCEST detection is not suitable for observing APT effect (19). Minimal contribution of glutamine to the GluCEST signal was demonstrated at 7T MRI scanner using phantoms containing 2 mmol/L (8) and 10 mmol/L glutamine (both phantoms pH ~7; Supplementary Fig. S3), respectively. Under our study conditions with tumor glutamine at 0.7 to 2.1 mmol/L range (Supplementary Table-S1) and pH ~7, glutamine contribution to GluCEST signal would be negligible. Second, owing to short treatment regimen (2-day) and specificity of CB-839 (3), which blocks conversion of glutamine to glutamate, the mobile protein concentration may remain unchanged while the change of

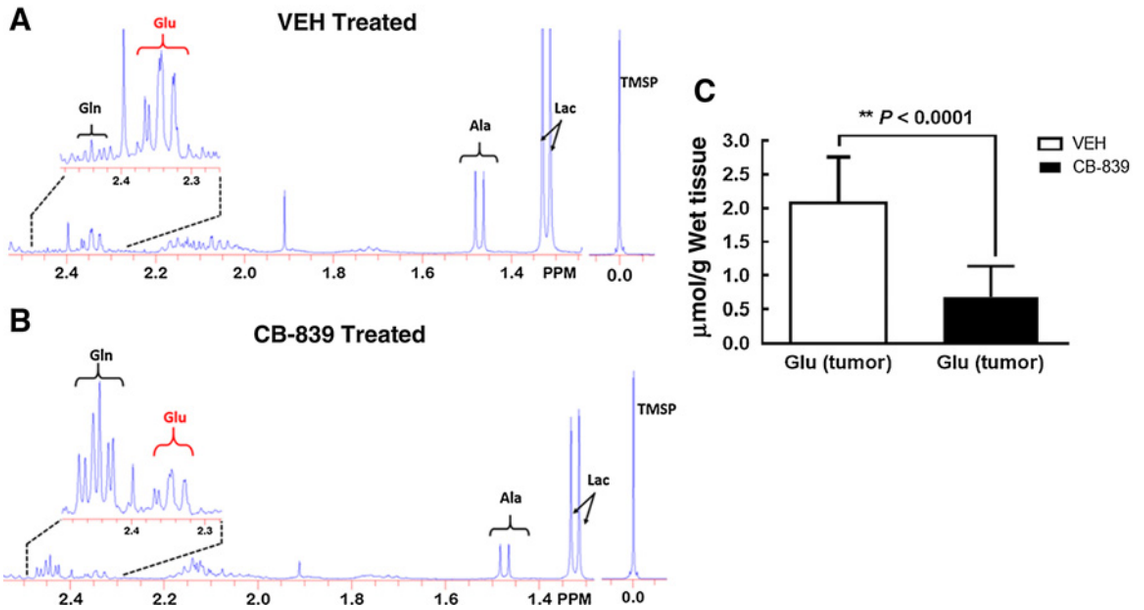

Figure 4.

Metabolites in perchloric acid–extracted tumor samples. Representative ^{1}H MR spectrum of the perchloric acid extract of the tumor from VEH (**A**)- and CB-839 (**B**)-treated mouse. Both spectra were scaled to the reference trimethylsilyl propanoic acid (TMSP) peak at 0 ppm. Insets, the H4 resonances of glutamate and glutamine. **C,** The tumor glutamate concentration (µmol/g of wet tissue) after four doses of VEH or CB-839 treatment. Glu, glutamate; Gln, glutamine; Ala, alanine; Lac, lactate.

glutamate concentration would have major contribution to the change of GluCEST asymmetry with modest contribution from Ala (Supplementary Table S1). Third, CB-839 lowered the tumor glutamate concentration by approximately 1.4 mmol/L corresponding to 2.5 percent points decrease in tumor GluCEST value, suggesting that each mmol/L change in glutamate concentration corresponds to 1.7 percent points change of the GluCEST value, consistent with the GluCEST sensitivity estimated in our previous study (20) plus modest contribution of Ala.

We have established a protocol that was insensitive to respiration motion and has robust test-retest repeatability (CV = 0.016), and as such, the 2.5 percent points reduction in GluCEST value after CB-839 treatment is reliable and significant (Fig. 3A). This absolute change represents 11.3% reduction from the baseline value ($P < 0.001$ compared with VEH controls). The minimal decrease of tumor pH_i (<1%, Fig. 3D) induced by CB-839 was not likely to impact the GluCEST value, but even it had, it would cause an increase of post-treatment GluCEST value, leading to an underestimation of the treatment effect. Meanwhile, a modest decrease (9.7%) in tumor Ala level (Supplementary Table S1) could have contributed to the overall reduction of GluCEST value mediated by *GLS* inhibition. Since Ala also exhibits GluCEST effect and the cellular glutamate and Ala pool are coupled via the alanine transferase (ALT) reaction (Fig. 1A), a decrease of Ala concentration accompanying the decrease of glutamate concentration would serendipitously increase the GluCEST sensitivity to *GLS* inhibition.

The change in the glutamate level in response to GLS inhibitor is much larger in cells (Fig. 1B) than in tumors (Fig. 4C), likely due to high drug concentration maintained in the culture media compared with mice in which rapid clearance and poor perfusion would certainly reduce tumor exposure to the drug. Our data revealed a relatively high baseline tumor GluCEST value of 18% ± 2% corresponding to a relatively low glutamate concentration in the tumor (2.1 ± 0.7 mmol/L), suggesting contributions of other amine protons. Compared with normal tissues such as the brain, proliferating tumors have a higher level of mobile proteins hence the associated amine protons could have contributed to the absolute GluCEST value. Therefore, it is not the absolute GluCEST value but its decrease that serves as a marker of GLS inhibition.

GLS inhibition results in a decrease of steady-state cellular glutamate concentration and an increase of glutamine concentration. Our earlier work has shown that PET imaging of [^{18}F](2S,4R)4-Fluoroglutamine, a glutamine analog, can detect changes of the tumor glutamine level induced by CB-839 (16). Because the glutamate-to-glutamine-ratio would better represent the degree of *GLS* inhibition and would be more sensitive than glutamate or glutamine alone, GluCEST MRI and Fluoroglutamine PET could be combined to optimally evaluate *GLS*-inhibiting drugs in future studies.

Our study has limitations. We examined a TNBC tumor model with relatively high GLS activity (3). Future studies should include a panel of TNBC lines with a range of GLS activities to further test the GluCEST utility. An intrinsic limitation of the GluCEST MRI is the requirement of high magnetic field (≥7 T) due to the intermediate exchange rate of the glutamate amine proton (9). Recent FDA approval of 7T MRI scanner will boost the applications of GluCEST, which has been successfully implemented to investigate human neurological/psychological diseases (11). Although challenges such as the presence of tumor microcalcification are expected, the clinical

application of GluCEST MRI may be motivated by its unique ability to assess cancer glutaminolysis and therapies targeting this metabolic signature.

Disclosure of Potential Conflicts of Interest

No potential conflicts of interest were disclosed.

Authors' Contributions

Conception and design: R. Zhou, D.A. Mankoff, R. Reddy
Development of methodology: R. Zhou, P. Bagga, H. Hariharan, R. Reddy
Acquisition of data (provided animals, acquired and managed patients, provided facilities, etc.): R. Zhou, P. Bagga, K. Nath, R. Reddy
Analysis and interpretation of data (e.g., statistical analysis, biostatistics, computational analysis): R. Zhou, P. Bagga, R. Reddy
Writing, review, and/or revision of the manuscript: R. Zhou, P. Bagga, H. Hariharan, D.A. Mankoff, R. Reddy
Administrative, technical, or material support (i.e., reporting or organizing data, constructing databases): R. Zhou, P. Bagga, R. Reddy
Study supervision: R. Zhou, R. Reddy
Other (performed *in vivo* 31p magnetic resonance spectroscopy): K. Nath

Acknowledgments

We thank Calithera for providing CB-839. We are grateful to Drs. Suzanne Wehrli, Susan Demo, and Hoon Choi and Jianbo Cao for technical assistance and helpful discussions. Technical support from the SAIF (Small Animal Imaging Facility) of Radiology Department is acknowledged. This study is supported by the National Institute of Biomedical Imaging and Bioengineering of the National Institutes of Health Grant P41-EB015893 (to R. Reddy), R01NS087516 (to R. Reddy), Abramson Cancer Center Breast Cancer Pilot Grant, BCPG2016 (to R. Zhou), R21CA198563 (to R. Zhou), R01CA211337 (to D. Mankoff and R. Zhou) and Komen SAC130060 (to D. Mankoff).

Received January 10, 2018; revised May 25, 2018; accepted July 30, 2018; published first August 2, 2018.

References

1. DeBerardinis RJ, Lum JJ, Hatzivassiliou G, Thompson CB. The biology of cancer: metabolic reprogramming fuels cell growth and proliferation. Cell Metab 2008;7:11–20.
2. Wang JB, Erickson JW, Fuji R, Ramachandran S, Gao P, Dinavahi R, et al. Targeting mitochondrial glutaminase activity inhibits oncogenic transformation. Cancer Cell 2010;18:207–19.
3. Gross MI, Demo SD, Dennison JB, Chen L, Chernov-Rogan T, Goyal B, et al. Antitumor activity of the glutaminase inhibitor CB-839 in triple-negative breast cancer. Mol Cancer Ther 2014;13:890–901.
4. Kung HN, Marks JR, Chi JT. Glutamine synthetase is a genetic determinant of cell type-specific glutamine independence in breast epithelia. PLoS Genet 2011;7:e1002229.
5. de Graaf RA. *In Vivo* NMR Spectroscopy—2nd Edition: Principles and Techniques. Hoboken, New Jersey: John Wiley & Sons, Ltd; 2007.
6. Begley JK, Redpath TW, Bolan PJ, Gilbert FJ. *In vivo* proton magnetic resonance spectroscopy of breast cancer: a review of the literature. Breast Cancer Res 2012;14:207.
7. Liu G, Song X, Chan KW, McMahon MT. Nuts and bolts of chemical exchange saturation transfer MRI. NMR Biomed 2013;26:810–28.
8. Cai K, Haris M, Singh A, Kogan F, Greenberg JH, Hariharan H, et al. Magnetic resonance imaging of glutamate. Nat Med 2012;18:302–6.
9. Crescenzi R, DeBrosse C, Nanga RP, Reddy S, Haris M, Hariharan H, et al. *In vivo* measurement of glutamate loss is associated with synapse loss in a mouse model of tauopathy. Neuroimage 2014;101:185–92.
10. Pepin J, Francelle L, Carrillo-de Sauvage MA, de Longprez L, Gipchtein P, Cambon K, et al. *In vivo* imaging of brain glutamate defects in a knock-in mouse model of Huntington's disease. Neuroimage 2016;139:53–64.
11. Davis KA, Nanga RP, Das S, Chen SH, Hadar PN, Pollard JR, et al. Glutamate imaging (GluCEST) lateralizes epileptic foci in nonlesional temporal lobe epilepsy. Sci Transl Med 2015;7:309ra161.
12. Ploessl K, Wang L, Lieberman BP, Qu W, Kung HF. Comparative evaluation of 18F-Labeled glutamic acid and glutamine as tumor metabolic imaging agents. J Nucl Med 2012;53:1616–24.
13. Baek S, Choi C-M, Ahn SH, Lee JW, Gong G, Ryu J-S, et al. Exploratory clinical trial of (4S)-4-(3-[18F]fluoropropyl)-l-glutamate for imaging xC−transporter using positron emission tomography in patients with non–small cell lung or breast cancer. Clin Cancer Res 2012;18:5427–37.
14. Singh A, Cai K, Haris M, Hariharan H, Reddy R. On B1 inhomogeneity correction of *in vivo* human brain glutamate chemical exchange saturation transfer contrast at 7T. Magn Reson Med 2013;69:818–24.
15. Kim M, Gillen J, Landman BA, Zhou J, van Zijl PC. Water saturation shift referencing (WASSR) for chemical exchange saturation transfer (CEST) experiments. Magn Reson Med 2009;61:1441–50.
16. Zhou R, Pantel AR, Li S, Lieberman BP, Ploessl K, Choi H, et al. [18F](2S,4R)4-Fluoroglutamine PET detects glutamine pool size changes in triple-negative breast cancer in response to glutaminase inhibition. Cancer Res 2017;77:1476–84.
17. Jones CK, Schlosser MJ, van Zijl PC, Pomper MG, Golay X, Zhou J. Amide proton transfer imaging of human brain tumors at 3T. Magn Reson Med 2006;56:585–92.
18. Vinogradov E, Sherry AD, Lenkinski RE. CEST: from basic principles to applications, challenges and opportunities. J Magn Reson 2013;229:155–72.
19. Jin T, Wang P, Zong X, Kim SG. MR imaging of the amide-proton transfer effect and the pH-insensitive nuclear overhauser effect at 9.4 T. Magn Reson Med 2013;69:760–70.
20. Bagga P, Pickup S, Crescenzi R, Martinez D, Borthakur A, D'Aquilla K, et al. *In vivo* GluCEST MRI: reproducibility, background contribution and source of glutamate changes in the MPTP model of Parkinson's disease. Sci Rep 2018;8:2883.